

# Accurate Real-Time Feedback of Surface EMG During fMRI

G. Ganesh, D. W. Franklin, R. Gassert, H. Imamizu and M. Kawato

*J Neurophysiol* 97:912-920, 2007. First published Sep 27, 2006; doi:10.1152/jn.00679.2006

**You might find this additional information useful...**

---

This article cites 30 articles, 9 of which you can access free at:

<http://jn.physiology.org/cgi/content/full/97/1/912#BIBL>

Updated information and services including high-resolution figures, can be found at:

<http://jn.physiology.org/cgi/content/full/97/1/912>

Additional material and information about *Journal of Neurophysiology* can be found at:

<http://www.the-aps.org/publications/jn>

---

This information is current as of May 15, 2007 .

# Accurate Real-Time Feedback of Surface EMG During fMRI

G. Ganesh,<sup>1,2</sup> D. W. Franklin,<sup>1,2</sup> R. Gassert,<sup>3</sup> H. Imamizu,<sup>2</sup> and M. Kawato<sup>2</sup>

<sup>1</sup>National Institute of Information and Communication Technology, Kyoto; <sup>2</sup>Advanced Telecommunication Research Institute Computational Neuroscience Laboratories, Kyoto, Japan; and <sup>3</sup>Laboratory of Robotic Systems, Ecole Polytechnique Fédérale de Lausanne, Lausanne, Switzerland

Submitted 6 June 2006; accepted in final form 24 September 2006

**Ganesh G, Franklin DW, Gassert R, Imamizu H, Kawato M.** Accurate real-time feedback of surface EMG during fMRI. *J Neurophysiol* 97: 912–920, 2007. First published September 27, 2006; doi:10.1152/jn.00679.2006. Real-time acquisition of EMG during functional MRI (fMRI) provides a novel method of controlling motor experiments in the scanner using feedback of EMG. Because of the redundancy in the human muscle system, this is not possible from recordings of joint torque and kinematics alone, because these provide no information about individual muscle activation. This is particularly critical during brain imaging because brain activations are not only related to joint torques and kinematics but are also related to individual muscle activation. However, EMG collected during imaging is corrupted by large artifacts induced by the varying magnetic fields and radio frequency (RF) pulses in the scanner. Methods proposed in literature for artifact removal are complex, computationally expensive, and difficult to implement for real-time noise removal. We describe an acquisition system and algorithm that enables real-time acquisition for the first time. The algorithm removes particular frequencies from the EMG spectrum in which the noise is concentrated. Although this decreases the power content of the EMG, this method provides excellent estimates of EMG with good resolution. Comparisons show that the cleaned EMG obtained with the algorithm is, like actual EMG, very well correlated with joint torque and can thus be used for real-time visual feedback during functional studies.

## INTRODUCTION

The advent of functional brain imaging modalities such as functional MRI (fMRI) and PET has allowed us to determine the specific brain areas involved in the production and control of motor tasks (Diedrichsen et al. 2005; Schaal et al. 2004; Shadmehr and Holcomb 1997). However, to fully understand motor control, it is critical to combine fMRI with techniques such as EMG, which give an estimate of the level of muscle activation. By examining the changes in muscle activity during adaptation to novel tasks, a deeper understanding of the mechanisms behind learning is obtained (Franklin et al. 2003b; Osu et al. 2003). The use of EMG to estimate the muscle activation is important because the brain does not simply control the force at the hand but also regulates the impedance of the limb during interactions with the environment (Burdet et al. 2001; Franklin et al. 2003a; Hogan 1984). Brain activation therefore is not only related to external variables such as kinematics or hand force, but is also related to other factors such as muscle force or muscle activation (Scott 2003; Todorov 2000). Furthermore, the acquisition of real-time EMG during functional imaging would allow for the accurate control of experiments using EMG feedback (Gomi and Osu 1998; Osu and Gomi 1999) in

the scanner. Better monitoring and control of individual muscle activation would greatly increase the variety of motor experiments possible during fMRI and the reliability of the results from these experiments. For example, this could enable experiments separating control of force from control of muscle co-contraction.

However, recording EMG data during fMRI is a technological challenge. Radio frequency (RF) pulses and magnetic field gradients, used during the imaging for excitation and spatial localization of the protons, induce large imaging artifacts in any EMG leads. Additionally, motor control studies may involve limb movements that result in movement artifacts as the EMG wires move in the magnetic field. It is necessary to suppress all of these artifacts to obtain measurable EMG from recordings during scanning. We examined the various methods proposed in literature to remove fMRI artifacts from EMG, as well as electroencephalography (EEG) signals. Most of these are postprocessing methods that are unsuitable for real-time artifact removal because they are either computationally expensive or require large averaging periods. Our objective is to develop a signal filtering system that is robust, computationally inexpensive, simple to implement, and enables good estimation of real-time EMG during fMRI.

Because of the large artifacts induced during scanning, one common strategy has been to completely avoid EMG recording during scanning. Several studies repeat the experiment outside the scanner to collect EMG, assuming that the EMG would be similar as when inside the scanner (Ehrsson et al. 2001; MacIntosh et al. 2004; Milner et al. 2005). Other studies use intermittent recording of EEG (Baudewig et al. 2001; Goldman et al. 2000) and EMG (Liu et al. 2000, 2002; Tanaka et al. 2004) during short intervals in between scans when the noise is low. This technique is able to provide a good estimate of EMG in experiments where the muscle activity is maintained at a constant level for a long time. However, if the muscle activity is intermittent, it becomes necessary to align the stimuli with the intervals in the scanning. This may be possible for fMRI experiments with a “blocked design,” but for “event-related designs,” requiring sparse sampling, alignment may reduce the population covered by the data points.

Among off-line processing methods, use of average artifact waveform subtraction is probably the most popular (Allen et al. 2000; Moosmann et al. 2003; Van Duinen et al. 2005). This method, however, requires de-synchronization of the stimuli and brain scans and a long averaging period, making on-line implementation difficult. High-frequency EEG acquisition dur-

Address for reprint requests and other correspondence: G. Ganesh, Computational Neuroscience Lab., ATR International, 2-2-2 Hikaridai, Seika-cho, Soraku-gun, Kyoto 619-0288, Japan (E-mail: gganesh@atr.jp).

The costs of publication of this article were defrayed in part by the payment of page charges. The article must therefore be hereby marked “advertisement” in accordance with 18 U.S.C. Section 1734 solely to indicate this fact.

ing fMRI is possible by customizing the echo-planar imaging (EPI) sequence to create short artifact-free periods (Anami et al. 2003). However, the customized and complex acquisition system reported still requires average artifact removal after acquisition before a clean signal is obtained. Other computationally intensive off-line methods include subtraction of an artifact template in the frequency domain (Sijbers et al. 1999) and temporal principle component analysis (Michiro et al. 2004).

A real-time artifact removal system reported for EEG (Garreffa et al. 2003) uses initial recordings of the MR artifact to determine the waveform of the EPI artifact for subtraction from subsequent EEG data. However, the higher frequency content of EMG, which requires precise signal synchronization, and changes in the artifact over time, could produce particular problems in adapting this technique for EMG recording.

It has been shown that the major part of the artifacts during fMRI using gradient-echo EPI are concentrated in particular frequencies and can be effectively reduced by removal of these frequencies from the signal (Hoffmann et al. 2000). However, the proposed method relies on postprocessing and has been used specifically to detect epileptic spikes in EEG that allow low-pass filtering below 40 Hz. We extend this method for real-time artifact removal in EMG that has a much larger frequency band (20–250 Hz) and hence larger artifact content. We propose an acquisition setup and a simple comb filter algorithm that enable real-time artifact removal from EMG during fMRI scanning. Comparisons with the EMG obtained from our algorithm with the noise-free EMG obtained in the absence of image artifacts show that the cleaned EMG is a very good estimate of the actual EMG. The proposed algorithm can work for both block and event-related fMRI without requiring any stimuli synchronization with the scanner or changes in the scanning protocol.

## METHODS

### Theory

The artifacts induced in the EMG lines can be classified as RF pulse artifacts, gradient field artifacts, and movement artifacts. The artifacts caused by the RF field (42.58 MHz/T for our scanner) are of much higher frequency than EMG and can be removed by low-pass filtering. In our case, we choose to use a separate RF filter to ensure that the RF noise does not saturate the input channels of the EMG amplifier. Gradient artifacts are induced by the gradient magnetic fields used during imaging for spatial encoding. The frequency range of the gradient field artifacts covers the entire EMG spectrum and thus cannot be removed by a low-pass filter and form the major part of the imaging artifacts in the EMG lines. The amplitude of the induced artifacts is given by Faraday's Law as

$$V_{\max} = \left( \frac{dB}{dt} \right)_{\max} \times A$$

where  $V_{\max}$  is the peak amplitude of the artifact,  $B$  is the magnetic field, and  $A$  represents the loop area. The maximum field gradient for our scanner is  $(dB/dt)_{\max} = 27 \text{ T s}^{-1}$  at a slew rate of  $72 \text{ T m}^{-1} \text{ s}^{-1}$ . Taking a conservative estimate for the loop area as  $10 \text{ cm}^2$ , we get a maximum gradient artifact of 54 mV (pk-pk) in the channels. In comparison, the amplitude of raw EMG is a few millivolts. Even though the noise magnitude is considerably higher than the raw EMG signal, the significant fact is that it is well below the input range of 500 mV of our EMG amplifier, which ensures that no part of the noise

signal is cut off during acquisition. Movement artifacts are induced because of the movement of the conductive loop formed by the electrodes and the neighboring wires in regions where the magnetic field is not uniform and caused by the change in the apparent loop area with the motion of the wires. The conductive loop is essentially fixed to the subject limb by the electrodes. Therefore as long as the wires are firmly fixed, the movement artifacts are in general concentrated around frequencies contained in the movement tasks, which rarely exceed 5 Hz. (In our present task, the artifacts were found to be below 3 Hz.) Presuming the movement artifacts are not large enough to saturate the input channels, they are removed effectively by high pass filtering of the data above 20 Hz.

During fMRI using gradient-echo EPI, the RF pulse and the gradient fields are applied repetitively to acquire image slices of the brain, with one complete brain volume (scan) acquired every repetition time (TR). Because of the nature of the scanning protocol, which repeats for every image slice, the imaging artifacts also repeat with a frequency equal to the slice acquisition frequency. The image sequence repeats every 98.6 ms (10.2 Hz) corresponding to the slice acquisition time (for a TR = 5 s). The sequence is very repeatable except for short periods in between every scan. A major chunk of the power in the noise is thus contained in the harmonics of the slice acquisition frequency (Fig. 1). The noise can thus be effectively reduced by removing these particular frequencies from the data (Hoffmann et al. 2000). We propose a linear comb filter for this purpose (see *Filter implementation*), which is easy to implement, computationally inexpensive, and can be thus implemented for real-time noise cancellation. Temporally concentrated interscan artifacts left over after the comb filtering operation are removed using a simple zero order hold on the output.

The signal is band-pass filtered between 20 and 250 Hz before passing into the comb filter. High-pass filtering above 20 Hz helps to remove movement artifacts and any temporal drifts present in the signal. Low-pass filtering below 250 Hz preserves most of the useful EMG data while reducing digitization errors, which increase with frequency and lead to clipping of signal peaks.

### EMG

In our setup, EMG was recorded from four muscles acting at the wrist [flexor carpi radialis (FCR), flexor carpi ulnaris (FCU), extensor carpi radialis longus (ECRL), and extensor carpi ulnaris (ECU)]. After electrode placements for each muscle were determined using functional movements, the area was cleansed with alcohol and abrasive gel (Nuprep, D.O. Weaver and Co.). EMG electrodes designed for use in the MR environment (NE-706A, Nihon Kohden) were filled with EEG electrode paste (Biotach, GE Marquette Medical Systems) and firmly fixed to the subjects skin with tape. Two electrodes were positioned on the belly of each muscle separated by ~1 cm. An elastic cloth sleeve was placed over the electrodes and wires, fixing them against the

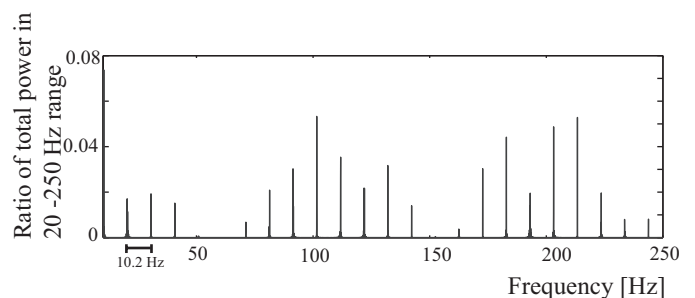


FIG. 1. Plot of power against frequency shows that noise is concentrated in frequencies in the multiple of 10.2 Hz, which corresponds to the slice acquisition frequency of our scanner during a scan of TR = 5 s. As we band-pass the incoming signal between 20 and 250 Hz before comb filtering, power has been expressed as a ratio of total power in this frequency range.

subjects forearm to avoid any accidental electrode removal and to minimize movements of the electrode wires during the scanning. Once the subject was positioned in the scanner, the long braided electrode wires were firmly fixed to prevent movement in the magnetic field. To avoid external noise being carried into the shielded MR room, the electrode wires were passed through multiple ferrite filters before passing through wave guides in the penetration panel of the MR room. The ferrite filters doubled up as filters for the high-frequency RF noise induced in the electrodes. The RF filtered signals were band-pass filtered between 20 and 250 Hz (−6 dB/octave, low-pass; −12 dB/octave, high-pass) and amplified using a Nihon Kohden filter-amplifier (MME-3132). The gain of each channel was adjusted to accommodate the complete noisy signal within the input range of the amplifier. The amplifier also contained a 60-Hz AC filter that could be switched on if required to remove any noise from the power-line used. All EMG equipment except for the electrodes and their wires were located outside of the scanning room.

Our primary concern was for the safety of the subjects during the experiments. The RF and gradient fields can induce large currents in the conducting loop formed by the subject, electrode wires, and amplifier. This was prevented by the large input impedance of our amplifier (~100 MΩ), narrow gauge of the MR electrode wires, and low-pass filtering at every input. Local capacitive loops between the electrode wires were prevented by the low capacitance (0.5 nF) of the MR-compatible electrodes wires. Furthermore, specially designed webbings on the MR electrodes helped to decrease eddy currents and prevent heating of electrodes during experiments.

After amplification, the signal was digitized at 5 kHz using a 12-bit AD converter (on a National Instruments PCI 6024E DAQ card). The artifact removal algorithm was implemented on a computer running xPC target real-time system. xPC Target environment uses a target PC, separate from a host PC, for running real-time applications. In our experiments, the target PC was used to run the cleaning algorithm while the host PC handled the visual display to the subjects.

*Filter implementation*

Let  $f(k)$  represent the  $k$ th real-time observation of the noisy signal after band-pass filtering between 20 and 250 Hz.  $f(k)$  is the summation of the EMG signal  $e(k)$  and EPI artifact,  $n(k)$

$$f(k) = e(k) + n(k) \tag{1}$$

The comb filter is implemented by a  $p$ th order difference equation and is represented in time space as

$$o(k) = \frac{(1 - B^p)}{2} f(k) \tag{2}$$

where  $o(k)$  is the output of the algorithm and  $B$  represents the backward shift operator such that  $B^p f(k) = f(k - p)$ . If  $t_s$  is the sampling time interval,  $f(k - p)$  represents value of  $f$ , observed  $pt_s$  seconds before  $f(k)$ . The value of  $p$  would be determined by the slice acquisition time  $t_a$  and sampling time  $t_s$  as  $p = t_a/t_s$ . Substituting from Eq. 1

$$o(k) = \frac{(1 - B^p)}{2} [e(k)] + \frac{(1 - B^p)}{2} [n(k)] \tag{3}$$

Because the artifacts are concentrated in the multiples of the slice acquisition frequency ( $w_a = 2\pi/t_a$ ) and the artifact waveform repeats with a time period equal to the slice acquisition time  $t_a$ , we have  $n(k) = n(k - p)$ . Therefore the second term in Eq. 3 tends to zero leading to artifact removal from the EMG signal. The effect of the filter on EMG signal  $e(k)$  is similar and EMG frequencies that are multiples of  $w_a$  are subjected to a gain of zero. The gain on the intermediate frequencies varies between zero and one (Fig. 2A).

The phase lag introduced by the filter is also shown in Fig. 2B. The phase lag, however, is not of major concern to us because the

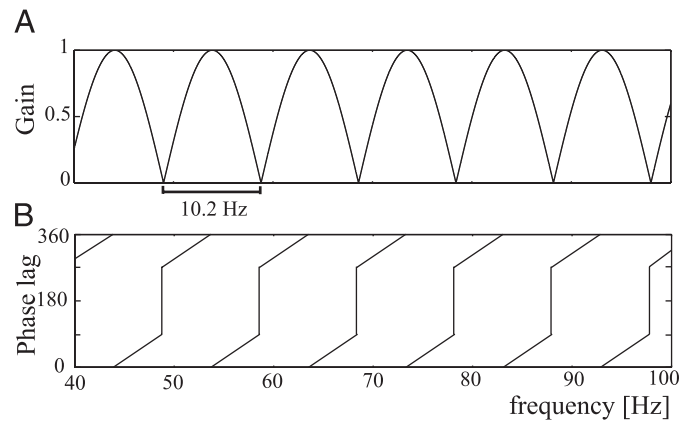


FIG. 2. Bode plot of comb filter. A: the simple comb filter implemented has a rectified sinusoidal gain profile. Frequencies in multiples of  $w_a$  are subjected to a gain of 0. Maximum gain of 1 is achieved on frequencies of  $(2n - 1)w_a/2$ . B: phase lag induced by filter.

cleaned EMG is rectified and integrated over a large moving window that is more than twice the maximum time lag introduced by the filter.

*Cleaning and visual feedback*

Even though the scanner noise is largely repetitive, the cycle is broken for a short period between scans. The artifacts during this interscan period are no longer concentrated in particular frequencies. Thus these interscan artifacts are not removed by the comb filter. However, these artifacts are temporally concentrated for a period of ~100 ms after each scan. By monitoring the sequence-related trigger of the MR system, it is possible to determine the exact period after every scan when this noise is present. To remove the interscan artifacts, data from the comb filter is subjected to a zero-order hold for a period of 200 ms after each scan. The hold value is taken as the average of the absolute cleaned EMG from a short period before the hold. While a shorter averaging period ensures better extrapolation of the current muscle activity, the chosen averaging period should be long enough to have an adequate number of data points to get a reliable average value. An average of 50 ms was chosen for our experiment, but a different period length may be chosen according to the experiment task. The cleaned EMG attained after passing through the comb filter, followed by interscan artifact removal, can now be smoothed as required for visual display. In our present setup (Fig. 3), we used a 500-ms moving average to obtain the EMG profile, corresponding to previous psychophysical on-line feedback studies (Gomi and Osu 1998; Osu and Gomi 1999). The EMG profile is monitored by the host PC at 20 Hz and can be used for real-time EMG feedback to the subject.

*Validation experiment*

Three healthy male subjects (23, 26, and 33 yr of age) participated in the experiment to validate the EMG cleaning algorithm. The institutional ethics committee approved the experiments and subjects gave informed consent before participation. A one degree of freedom MR compatible interface (Gassert et al. 2006) was used to restrain the subject's forearm and wrist to an isometric posture using a plastic splint and straps while the subject contracted his muscles (Fig. 4). This device also contained a custom MR-compatible optical torque sensor that was used to collect wrist joint torque during the experiment.

The experiment consisted of isometric wrist contractions in both the flexion and extension direction during scanning. The subject's hand was firmly fixed to the handle of the MR compatible manipulandum.

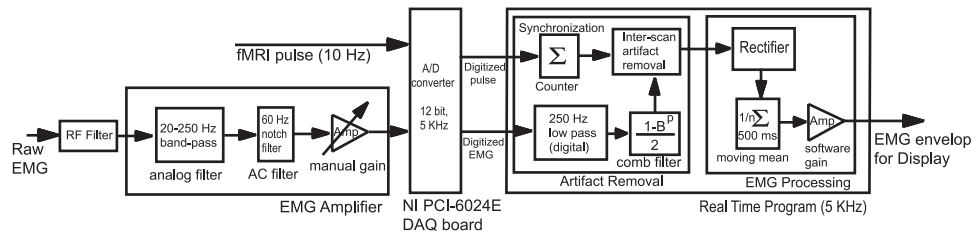


FIG. 3. Block diagram of setup used to acquire real-time EMG during functional MRI (fMRI). Raw EMG signal collected during scanning is contaminated with imaging artifacts. The raw EMG is radio frequency (RF) filtered and passed into a commercial EMG amplifier where it is band-pass filtered between 20 and 250 Hz, AC filtered to remove noise from power supply, and amplified before being passed into the artifact removal program through a data acquisition (DAQ) board. A pulse sequence acquired from the scanner (fMRI pulse) is also fed in through the DAQ board to synchronize the program with the scanner. Comb filter and interscan artifact removal are implemented at 5 kHz. Cleaned EMG acquired after interscan artifact removal is rectified and averaged over a 500-ms moving window to obtain the EMG envelope for visual display.

Subjects were presented with visual feedback of the torque applied to the manipulandum in the form of a torque bar whose length and direction indicated the magnitude and direction of the applied torque. One of three flexion and three extension target torque levels ( $\pm 7$  Nm maximum) were displayed in a random order every 10 s. The subject was instructed to slowly increase the torque bar to the target level in  $\sim 1$ – $2$  s and hold it throughout the target display period. Once a new target appeared, subjects initially relaxed for a period of 1 s and then slowly produced enough torque to match the new torque target. Each target level was presented four times during one session. All experiments were performed both with and without functional imaging. These two experiments were performed one following the other, without moving the subject or electrodes so that a direct comparison of the EMG signal can be made. A short rest period of 3–4 min was provided between experiments to ensure that the subject was not fatigued.

A big advantage of this technique for obtaining an on-line measure of EMG compared with other methods such as interleaved EMG recording (Tanaka et al. 2004) is that this technique is able to obtain information about continuously changing EMG levels throughout the scanning. To show this ability, an additional session was performed with one subject, where the subject was asked to make quick flexion and extension wrist torques in the isometric condition without maintaining a constant force level as in the previous experiment. The torque values in this session were constantly changing and usually lasted  $\sim 3$  s before changing directions, for example, from flexion to extension. Data from this experiment were used to check the algorithm's performance for higher activation frequencies.

**fMRI**

A 1.5-T MR scanner (Shimadzu-Marconi ECLIPSE 1.5T Power Drive 250) was used to obtain blood oxygen level-dependent

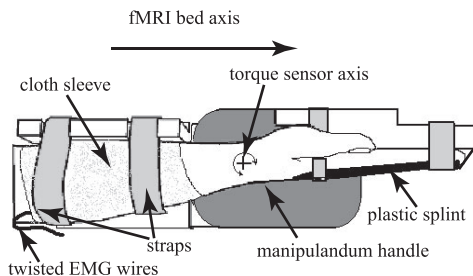


FIG. 4. Arm fixation during validation experiment. Subject's forearm and wrist were fixed to the handle of the MR compatible manipulandum using Velcro straps and a hard plastic splint. An elastic cloth sleeve was put over subject's forearm to prevent accidental removal of electrodes and minimize wire movement during experiment. Axis of the MR compatible torque sensor (located below subject hand) was aligned with axis of rotation of the wrist. Subject performed isometric flexion and extension contractions of the wrist in this setup.

(BOLD) contrast functional images. Images weighted with the apparent transverse relaxation time were obtained with an gradient-echo EPI sequence. Data were collected at two different repetition times of 1) TR = 2.5 s with echo time, 49 ms; flip angle, 80°, 25 slices (thickness 4 mm, gap 2 mm) of  $64 \times 64$  in plane voxels (in-plane field of view of 224 mm<sup>2</sup>) and 2) TR = 5 s with echo time, 50 ms; flip angle, 90°, 50 slices (thickness 3 mm) of  $64 \times 64$  in plane voxels (in-plane field of view of 224 mm<sup>2</sup>).

In a control session, additional fMRI images were collected in the absence of the EMG setup but with similar imaging parameters. The control session was conducted immediately after one of the EMG sessions to ensure that a direct contrast between the brain images was possible. Data collected in the EMG and control sessions were realigned to the first volume of the EMG session, normalized to the Montreal Neurological Institute (MNI) reference brain, and smoothed using an 8-mm full-width half-maximum Gaussian kernel. The T-contrasts ( $P < 0.05$ , FDR corrected, 0-voxel threshold) of the active and rest phases in each of the two sessions was performed and compared with observations reported in literature for wrist muscle activations. A T-contrast ( $P < 0.001$ , uncorrected, 0 voxel threshold) of the brain images from the active phases of the EMG and control sessions was conducted to check for possible imaging artifacts caused by the EMG setup.

**Analysis**

To evaluate the accuracy of the algorithm, analysis of the cleaned EMG data was performed and compared with data recorded in the absence of fMRI scanning. The goal of this technique was to produce an accurate on-line estimate of the EMG during the scanning. Therefore the critical test of the data are whether the cleaned EMG exhibits good correlation with actual artifact-free EMGs. However, a direct correlation between the two integrated EMG signals was not possible because there can be differences in the force levels and muscle activation patterns between trials. Second, because the power of the EMG signal is reduced by the filtering in the cleaning algorithm, the overall level of the muscle activity after cleaning is lower than what is recorded without MR scanning. Thus we choose to check the correlation between the EMG signals by correlating them individually with the corresponding signals from the joint torque sensor because this is invariant to the MR scanning. EMG has been shown to increase as a function of joint torque in either a linear or nonlinear fashion depending on the muscles studied (Gottlieb and Agarwal 1971; Lawrence and De Luca 1983; Milner-Brown et al. 1973; Woods and Bigland-Ritchie 1983). For smaller distal muscles and lower joint torque or force levels, this relationship is generally found to be linear, although at higher forces, for more proximal muscles the EMG can increase at a faster rate than the muscle force. In this study, we wished to confirm that the cleaned EMG is a good estimate of the underlying motor command. In particular, we tested this by examining whether the cleaned EMG scales with joint torque during isometric contrac-

tions was similar to EMG recorded without the MR scanning. If both exhibit a linear relation with the joint torque, we can conclude that the cleaned EMG is well correlated to the actual muscle activity. A 500-ms moving window was used to calculate the integrated, rectified EMG. The mean integrated value over 2.5 s at the beginning of each session when no torque was applied was used to estimate the zero-offset. This offset was subtracted from the integrated EMG values. This integrated EMG value was compared with the measured wrist torque every 250 ms for EMG recorded with and without fMRI scanning.

The data for each muscle were plotted against joint torque and linear regression against joint torque was performed for flexion and extension directions separately. The correlation coefficient ( $r^2$ ) was used to determine the extent to which the EMG measure was correlated with joint torque for sessions both with and without scanning. Best-fit lines were calculated using linear regression to examine the way in which the muscle activity scaled with joint torque.

For graphing purposes, the data for each muscle were collected across all of the trials. The EMG values were separated into 12 equally sized bins depending on the joint torque level recorded at that time. For each bin, the mean and standard deviation of the data were determined and plotted at the location of the mean joint torque for the bin.

RESULTS

Before cleaning was performed, the EMG signal largely consisted of imaging artifacts from the scanner (Fig. 5A). After

passing through the comb filter, a majority of the image artifacts were removed. The EMG can already be seen in the signal (Fig. 5B), but it is still corrupted by interscan artifacts. The interscan artifacts were concentrated over a period of ~100 ms and repeated after time intervals corresponding to the TR of the scan. The signal after removal of the interscan artifacts (Fig. 5C) looks very similar to the artifact-free (no-fMRI) EMG (Fig. 5D). Figure 5E shows the corresponding torque profile over the same time period. On zooming in to a smaller time interval (Fig. 5F), the cleaned and actual EMG still look similar but at this scale, the lower density of the cleaned EMG, because of removal of part of the EMG power, is clearly visible. Also visible at the higher magnification is the 200-ms hold used to remove the interscan artifacts. The lower density of the cleaned signals leads to a lower integrated value for the cleaned EMG in comparison with the actual EMG (Fig. 5G).

The mean EMG was compared against corresponding joint torque. The correlation coefficients  $r^2$  for the cleaned EMG and no-fMRI EMG for all the subjects and muscles are given in Table 1. In one subject, the ECU muscles showed very low signal to noise ratio in recordings without scanning and was therefore not recorded during scanning. The plot of mean EMG against torque for one flexor and one extensor muscle for each

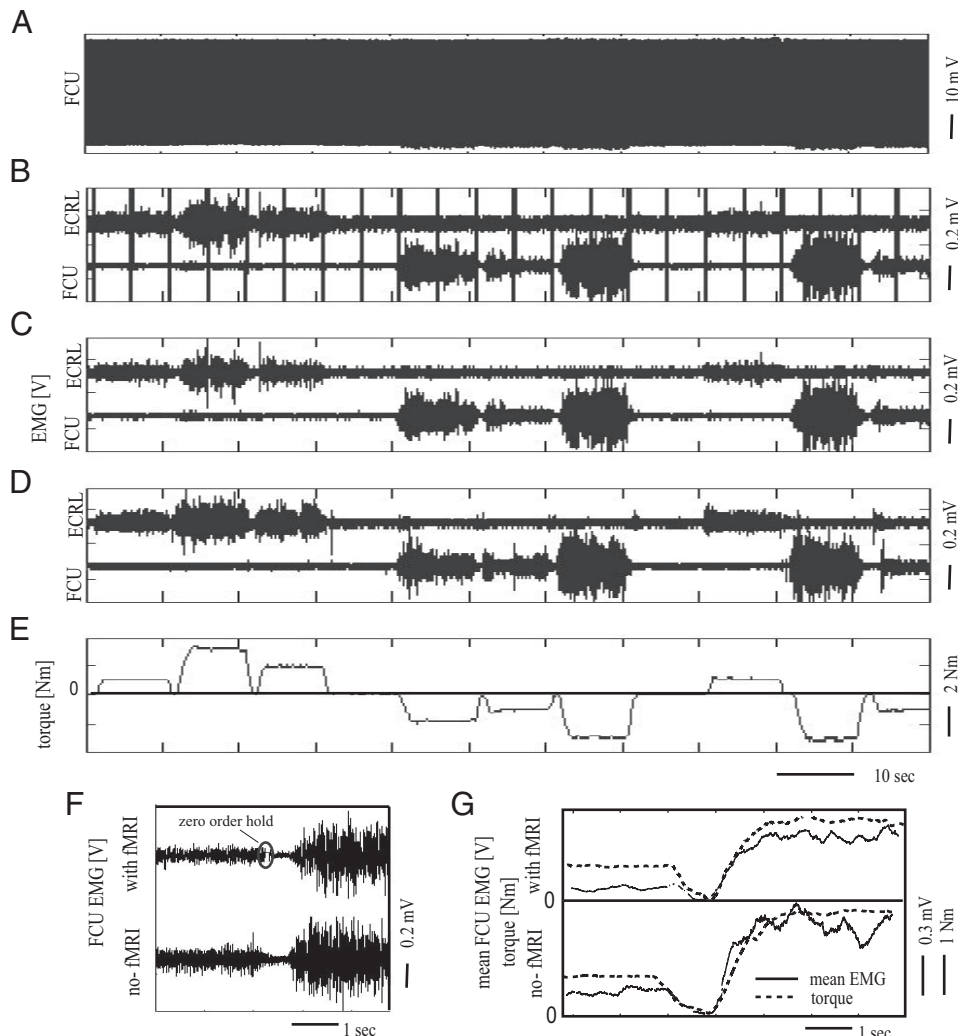


FIG. 5. Comparison of cleaned and no-fMRI EMG. A: signal in FCU channel after the application of band-pass filter of 20–250 Hz is contaminated by artifacts. B: 2 EMG channels: 1 flexor (FCU) and 1 extensor (ECRL) for *subject 1*, after passage through the comb filter shows EMG profile clearly. EMG is still contaminated by interscan artifacts, which are seen as thick vertical lines in the figure, repeat every 5 s, corresponding to the TR of this session. C: the same channels, after removal of interscan artifacts, show very good similarity to (D) EMGs collected in the absence of scanning over the same time period. E: torque value from torque sensor. Note that extensor and flexor muscle activities correspond to positive and negative torque values, respectively. F: time-magnified view of flexor carpi radialis (FCR) activity after artifact removal compared with activity of the same muscle in the absence of scanning shows the 200-ms hold period (highlighted) used to remove interscan artifacts. However, cleaning decreases power content of EMG signals, which is apparent in G, where a 500-ms moving average is applied on rectified EMG signals.

TABLE 1. Results of correlation between mean muscle activity and joint torques for three subjects

Subject	$r^2$							
	FCU		ECRL		FCR		ECU	
	Cleaned EMG	No-fMRI EMG	Cleaned EMG	No-fMRI EMG	Cleaned EMG	No-fMRI EMG	Cleaned EMG	No-fMRI EMG
1	0.816	0.916	0.791	0.918	0.742	0.795	0.642	0.798
2	0.798	0.857	0.914	0.913	0.667	0.806	—	—
3	0.718	0.955	0.763	0.914	0.483	0.807	0.470	0.889

Values are  $r^2$ . FCU, flexor carpi ulnaris; ECRL, extensor carpi radialis longus; FCR, flexor carpi radialis; ECU, extensor carpi ulnaris.

of the three subjects is shown in Fig. 6. Clearly both the cleaned EMG and the EMG recorded without scanning exhibited linear relationships with either the negative or positive torque depending on the action of the muscle, thus showing good correlation between cleaned and the no fMRI (actual) EMG. The initial trials were performed with large target torque range ( $\pm 7$  Nm) and therefore large muscle activity. To confirm that the method works well over all ranges of muscle activity,

a smaller torque range ( $\pm 1.5$  Nm) was also used with two of the subjects. Over this smaller torque range, the cleaned EMG still shows a linear response to joint torque with large  $r^2$  values (Fig. 6, B and C). To show that the algorithm works for scanning with different TR, an additional session was conducted for *subject 1* with a TR = 2.5 s and two muscles (FCU and FCR). This gave ( $r^2_{\text{cleaned}}$ ;  $r^2_{\text{no fMRI}}$ ) values of (0.773; 0.916) and (0.473; 0.640), respectively. For the same subject, muscles ECU and ECRL were recorded during the session with higher frequency activations of  $\sim 1$ –1.5 Hz and gave  $r^2$  values of (0.637; 0.796) and (0.832; 0.928), respectively. Again both the no fMRI EMG and the cleaned EMG exhibited linear relations with joint torque and had large  $r^2$  values. Figure 7A shows the torque and the integrated cleaned EMG profile for the ECRL muscle during this session. The torque EMG regression for the same muscle is shown in Fig. 7B.

Experiments performed in the control session, in the absence of the EMG setup, showed similar brain activations as in the sessions with EMG (Fig. 8, A and B). Activation was observed in parts of the left motor cortex including M1 and the premotor regions, SMA and in the right cerebellum, in agreement with the literature on activation of the muscles in the right hand (Kawashima et al. 1995; Milner et al. 2005). Furthermore, the

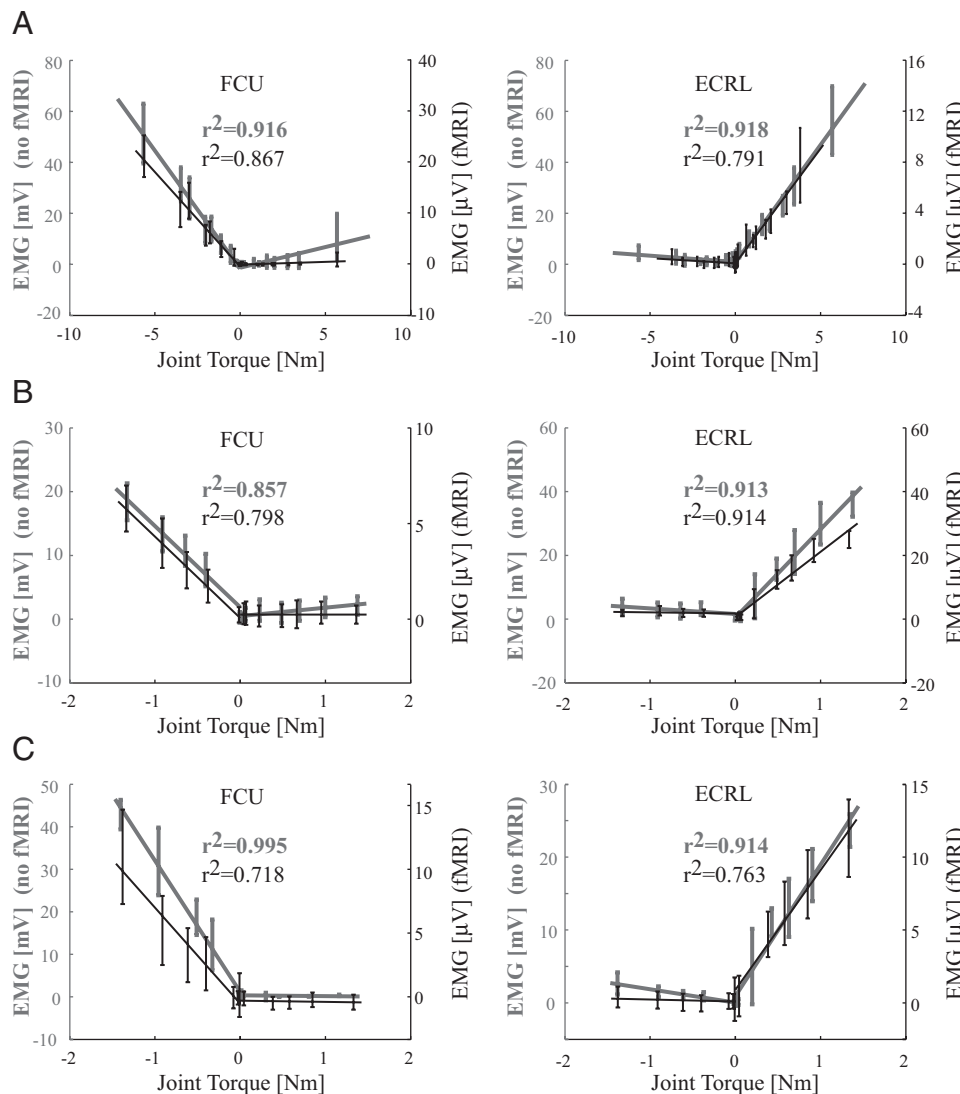


FIG. 6. Cleaned EMG scales with joint torque like normal EMG. A: EMG recorded without scanning (thick grey trace) and cleaned EMG recording during scanning (thin black trace) plotted as a function of wrist joint torque for *subject 1*. Wrist flexor (FCU; left) increases activity as wrist flexion increases, whereas wrist extensor (ECRL; right) increases activity as the extensor torque required is larger. Muscle activity has been separated into 2 groups depending on whether the joint torque was an extensor torque or a flexor torque. Each group was fitted by a line using linear regression (least squares error). Resulting best-fit lines are shown with solid lines. Error bars indicate SD of equal-sized groups of actual EMG values. Above each plot is the  $r^2$  value shown only for the region where the muscle is active (flexion region for flexor muscles; extensor region for extensor muscle). B: data from the same muscles for *subject 2* and (C) *subject 3* show that linearity of mean EMG with joint torque is maintained even for low levels of joint torques.

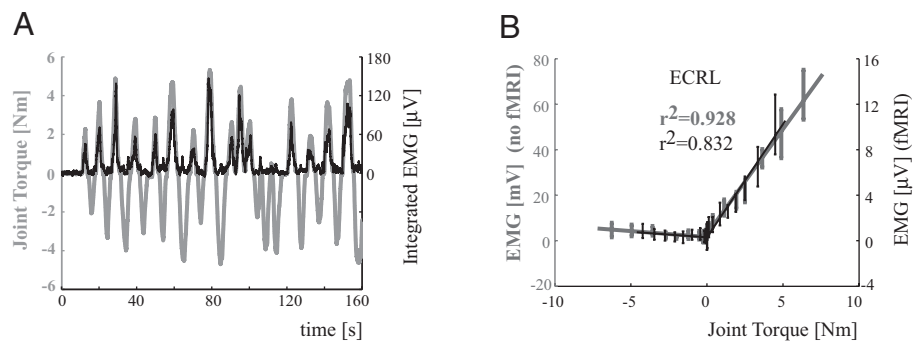


FIG. 7. Cleaning technique can handle quickly changing EMG activity. *A*: subject was instructed to make quickly changing isometric flexion and extension torques (thick grey trace). Cleaned EMG was recorded, and the 500-ms moving window of integrated EMG was calculated during recording (thin black trace). ECRL muscle is an extensor muscle so it was only active when an extensor torque (positive joint torque) was produced. *B*: integrated EMG plotted against joint torque for these fast contractions. Cleaned EMG (thin black trace) scales with joint torque exactly as does normal EMG (thick grey trace) recorded without scanning. Data are plotted as in Fig. 6.

contrast of the brain images from the active phases of the EMG and control sessions gave no significantly active voxels even at a low threshold ( $P < 0.001$ , uncorrected, 0-voxel threshold; Fig. 8C). Thus it was concluded that the EMG system is compatible with the scanner and does not induce any significant noise in the brain images.

DISCUSSION

Our work shows that a simple comb filter can provide real-time noise reduction in EMG signals during fMRI scanning with minimum complication. Comparison with artifact-free EMG collected in the absence of scanner noise showed good similarity between the EMG profiles between the two, even when viewed over a shorter time period (Fig. 5, C, D, and F). The cleaned integrated EMG linearly scaled with torque, similar to EMG recorded without scanner noise (Fig. 6), hence also showing that cleaned EMG has a good correlation to the underlying muscle activation over a wide range of levels. This

was further supported by evidence that the algorithm can even detect activity during weak contractions ( $\leq 0.3$  Nm). These properties suggest that the cleaned EMG resulting from the algorithm can be used for providing EMG feedback during fMRI experiments.

In our present prototype system, we used a simple linear filter for noise removal. The simplicity of the filter makes it easy to implement, computationally inexpensive, and easy to realize for real-time applications. However, the gain profile of filter removes parts of the EMG spectrum (Fig. 2), leading to a loss of  $\sim 35\%$  of the EMG spectrum in theory. Thus for experiments involving EMG spectral analysis, other off-line cleaning methods are recommended. In the future, nonlinear comb filters may be implemented with sharper gain profiles to reduce the spectrum loss considerably. On the other hand, even with the simple linear filter, the output cleaned EMG looks very good because of the fact that the EMG power spectrum is relatively smooth and there are no sudden changes in the power content across neighboring frequencies. Thus even with the loss of a relatively large percentage of the spectrum the algorithm is able to capture the EMG waveform well. The loss in power is apparent in the y-axis labels of the results figures where the integrated cleaned EMG is always less than the normal EMG for a given level of joint torque. However, this is simply a scaling down of the EMG level and does not affect the ability to detect the muscle activity itself. The variability of the EMG, as indicated by the SD of the values (Fig. 6), is similar both with and without scanning, relative to the mean value of the EMG.

Even though it was expected that the ratio of the slopes of the cleaned and no fMRI EMG would be same for all channels, this was found not to be so in practice (Fig. 6). This was because, although the major part of the noise is concentrated in the slice frequency harmonics and is removed by the algorithm completely, there is some noise present in the frequencies adjacent to the harmonic frequencies that is attenuated but not completely removed. This residual noise varies within channels depending on their individual spatial placements and leads to differences in the slopes of the integrated cleaned EMG in Fig. 6. However, the noise, and hence the slopes, remains the same as long as the position of the subject was not changed, as seen from Fig. 6A and Fig. 7B, where the same muscle is plotted in two different sessions.

The order of the digital filter is extremely important for the good performance of the algorithm. This order is determined by the slice acquisition time ( $t_a = TR/\text{number of slices}$ ) and hence the time period of the noise cycle. Commonly specified TR values are usually rounded off to the nearest half second.

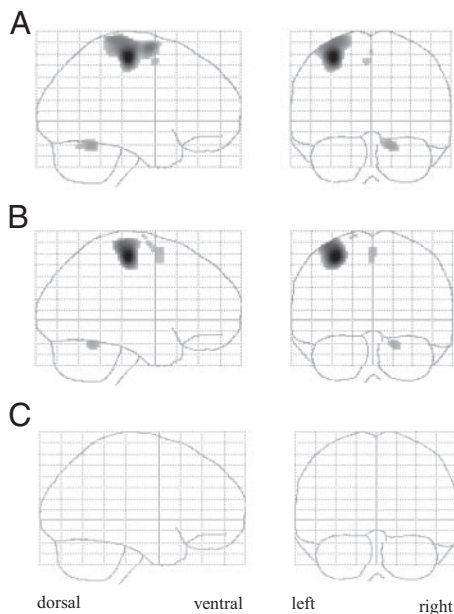


FIG. 8. Brain activity during EMG acquisition. Contrast of brain activity during the active and rest phases ( $P < 0.05$ , FDR corrected) of a subject in (A) the session with EMG and (B) in the control session without the EMG setup shows very similar activity. Activations were observed in parts of the left M1, premotor, SMA, and right cerebellum corresponding to observations reported in literature. *C*: contrast of the active phases of the 2 sessions gave no significant activity even at a low threshold of  $P < 0.001$ , uncorrected, 0 voxel threshold. This showed that EMG setup does not indicate any artifacts in fMRI images.

However, because of the preparation time taken by some scanners, the actual TR during scanning is 60–70 ms (70 ms for our scanner) less than the specified TR value. This leads to a difference of 2–3 ms in  $t_a$ . Because of the large magnitude of the artifacts, this small error can reduce the signal to noise ratio of the cleaned EMG significantly. We thus provide the possibility of fine-tuning the filter order on-line during EMG collection.

The interscan artifact are removed using a zero order hold for every 200 ms between scans. EMG during this period is estimated from the previous 50 ms. Again this method was used in the prototype system because it is simple to implement. However, more accurate methods like mean waveform subtraction may be used for this period because the frequency content of the interscan artifact is low. Furthermore, during a major part of the interscan period, the artifacts are negligible, and clean EMGs can be obtained without any artifact filter (Liu et al. 2000, 2002). The RF artifact magnitude varied between channels, possibly because of the positioning of the electrode. In some of the channels, an additional zero-order hold during the period when the RF noise is present (in our setup, the 1st 25 ms of a slice acquisition) improved the signal to noise ratio significantly, especially when the EMG values were low.

Movement artifacts are induced by the movement of the electrodes and wires in the magnetic field. In isometric experiments, both single and multi-joint, these artifacts originate from the small movement of the skin and the limb on which the electrodes are fixed and are generally small in magnitude. Among non-isometric experiments involving limb movements, wrist and finger experiments produce less artifacts as there is little movement of the forearm where the electrodes are fixed. However, in the case of multi-joint movements, artifacts can be larger in magnitude and frequency. To minimize movement artifacts, EMG wires should be fixed and run along limbs and the fMRI bed without forming any loops near the scanner. The workspace of the experiment should be made as small as possible and should be located as close as possible to the axis of the bed and the center of the scanner bore, where the magnetic field is more uniform. Generally speaking, the movement frequency content in most of the motor tasks is <5 Hz and a high pass cut-off of >20 Hz should be sufficient to remove movement artifacts. However, for motor tasks involving sudden obstacles and perturbations, a higher cut-off frequency may be chosen if required. Note that the algorithm is able to remove the movement artifacts provided the input channels are not saturated. An EMG amplifier with a large input range is thus preferred for multi-joint movement studies.

Even though we collect EMG in a 1.5-T scanner, present day experiments often use EPI at 3-T for human subjects. However because EPI principally involves repetitive application of magnetic fields, the noise is always concentrated in the harmonics of the slice acquisition frequency of the scanner. Thus with proper tuning of the filter order, the algorithm can be effectively used for stronger scanners as well.

Visual feedback of the EMG can enable monitoring and control of individual muscles during motor experiments. Because of the redundancy in the human muscle system, this is not possible from recordings of joint torque and kinematics alone, which contain no information about muscle co-contractions. Proper control of muscle activation is critical during brain imaging, because brain activation is likely to change as

muscle activation varies. Control of individual muscle activation can therefore increase the variety of motor experiments possible during fMRI and increase the reliability and repeatability of the results obtained. Using the proposed setup and algorithm, we have shown for the first time that real-time acquisition of EMG signals during fMRI is possible, opening up a new experimental design paradigm in the MR scanner: the conduction of motor experiments that use feedback of muscle activity to control the actions of the subject.

#### ACKNOWLEDGMENTS

We thank Dr. Theodore Milner at Simon Fraser University and Drs. Masahiko Haruno and Eiichi Naito at Advanced Telecommunication Research Institute for valuable comments.

#### GRANTS

This study was supported in part by the National Information and Communications Technology (NICT-KARC) and by grants to M. Kawato from the Human Frontier Science Program (HFSP).

#### REFERENCES

- Allen PJ, Josephs O, Turner R.** A method for removing imaging artifact from continuous eeg recorded during functional mri. *Neuroimage* 12: 230–239, 2000.
- Anami K, Mori T, Tanaka F, Kawagoe Y, Okamoto J, Yarita M, Ohnishi T, Yumoto M, Matsuda H, Saitoh O.** Stepping stone sampling for retrieving artifact-free electroencephalogram during functional magnetic resonance imaging. *Neuroimage* 19: 281–295, 2003.
- Baudewig J, Bittermann HJ, Paulus W, Frahm J.** Acquiring simultaneous eeg and functional mri. *Clin Neurophysiol* 112: 1196–1200, 2001.
- Burdet E, Osu R, Franklin DW, Milner TE, Kawato M.** The central nervous system stabilizes unstable dynamics by learning optimal impedance. *Nature* 414: 446–449, 2001.
- Diedrichsen J, Hashambhoy Y, Rane T, Shadmehr R.** Neural correlates of reach errors. *J Neurosci* 25: 9919–9931, 2005.
- Ehrsson HH, Fagergren A, Forssberg H.** Differential fronto-parietal activation depending on force used in a precision grip task: an fmri study. *J Neurophysiol* 85: 2613–2623, 2001.
- Franklin DW, Burdet E, Osu R, Kawato M, Milner TE.** Functional significance of stiffness in adaptation of multijoint arm movements to stable and unstable dynamics. *Exp Brain Res* 151: 145–157, 2003a.
- Franklin DW, Osu R, Burdet E, Kawato M, Milner TE.** Adaptation to stable environments achieved by combined impedance control and inverse dynamics model. *J Neurophysiol* 9: 3270–3282, 2003b.
- Garreffa G, Carni M, Gualniera G, Ricci GB, Bozzao L, Carli DD, Morasso P, Pantano P, Colonnese C, Roma V, Maraviglia B.** Real-time mr artifacts filtering during continuous eeg/fmri acquisition. *Magn Reson Imaging* 21: 1175–1189, 2003.
- Gassert R, Moser R, Burdet E, Bleuler H.** MRI/fMRI-compatible robotic system with force feedback for interaction with human motion. *IEEE/ASME Trans Mechatron* 11: 216–224, 2006.
- Goldman RI, Sternb JM, Engel J Jr, Cohen MS.** Simultaneous eeg and functional mri of epileptic activity: a case report. *Clin Neurophysiol* 111: 1974–1980, 2000.
- Gomi H, Osu R.** Task-dependent viscoelasticity of human multijoint arm and its spatial characteristics for interaction with environments. *J Neurosci* 18: 8965–8978, 1998.
- Gottlieb GL, Agarwal GC.** Dynamic relationship between isometric muscle tension and the electromyogram in man. *J Appl Physiol* 30: 345–351, 1971.
- Hoffmann A, Jager L, Werhahn KJ, Jaschke M, Noachtar S, Reiser M.** Electroencephalography during functional echo-planar imaging: detection of epileptic spikes using post-processing methods. *Magn Reson Med* 44: 791–798, 2000.
- Hogan N.** Neural, mechanical and geometric factors subserving arm posture in humans. *J Neurosci* 4: 2745–2754, 1984.
- Kawashima R, Itoh H, Ono S, Satoh K, Furumoto S, Gotoh R, Koyama M, Yoshioka S, Takahashi T, Yanagisawa T.** Activity in the human primary motor cortex related to arm and finger movements. *Neuroreport* 6: 238–240, 1995.
- Lawrence JH, De Luca CJ.** Myoelectric signal versus force relationship in different human muscles. *J Appl Physiol* 54: 1653–1659, 1983.

- Liu J, Daib TH, Elsterb TH, Sahgal V, Brown RW, Yue GH.** Accessory hardware for neuromuscular measurements during functional MRI experiments. *Magn Res Mat Phys Biol Med* 13: 164–171, 2000.
- Liu J, Zhang L, Yao B, Yue GH.** Simultaneous measurement of human joint force, surface electromyograms, and functional mri-measured brain activation. *J Neurosci Methods* 101: 49–57, 2002.
- MacIntosh BJ, Mraz R, Baker N, Tam F, Staines WR, Graham SJ.** Optimizing the experimental design for ankle dorsiflexion fmri. *Neuroimage* 22: 1619–1627, 2004.
- Michiro N, Abildgaard M, Nixon T, Constable RT.** Removal of time-varying gradient artifacts from eeg data acquired during continuous fmri. *Clin Neurophysiol* 115: 2181–2192, 2004.
- Milner TE, Franklin DW, Imamizu H, Kawato M.** Central representation of dynamics when manipulating handheld objects. *J Neurophysiol* 95: 893–901, 2005.
- Milner-Brown HS, Stein RB, Yemm R.** The orderly recruitment of human motor units during voluntary isometric contractions. *J Physiol* 230: 359–370, 1973.
- Moosmann M, Ritter P, Krastel I, Brink A, Thees S, Blankenburg F, Taskin B, Obrig H, Villringer A.** Correlates of alpha rhythm in functional magnetic resonance imaging and near infrared spectroscopy. *Neuroimage* 20: 145–158, 2003.
- Osu R, Burdet E, Franklin DW, Milner TE, Kawato M.** Different mechanisms involved in adaptation to stable and unstable dynamics. *J Neurophysiol* 9: 3255–3269, 2003.
- Osu R, Gomi H.** Task-dependent viscoelasticity of human multijoint arm and its spatial characteristics for interaction with environments. *J Neurophysiol* 81: 1458–1468, 1999.
- Schaal S, Sternad D, Osu R, Kawato M.** Rhythmic arm movement is not discrete. *Nat Neurosci* 7: 1137–1144, 2004.
- Scott SH.** The role of primary motor cortex in goal-directed movements: insights from neurophysiological studies on non-human primates. *Curr Opin Neurobiol* 13: 671–677, 2003.
- Shadmehr R, Holcomb HH.** Neural correlates of motor memory consolidation. *Science* 277: 821–825, 1997.
- Sijbers J, Michiels I, Verhoyle M, Van Audekerke J, Van der Linden A, Van Dyck D.** Restoration of mr-induced artifacts in simultaneously recorded mr/eeg data. *Magn Reson Imaging* 17: 1383–1391, 1999.
- Tanaka Y, Noda S, Tsuji T.** A virtual prosthetic hand using EMG signals for fMRI measurements. International Conference on Intelligent Robots and Systems IROS, September 28–October 2, 2004, Sendai, Japan.
- Todorov E.** Direct cortical control of muscle activation in voluntary arm movements: a model. *Nat Neurosci* 3: 391–398, 2000.
- Van Duinen H, Zijdwind I, Hoogduin H, Maurits N.** Surface emg measurements during fmri at 3t: accurate emg recordings after artifact correction. *Neuroimage* 27: 240–246, 2005.
- Woods JJ, Bigland-Ritchie B.** Linear and non-linear surface EMG/force relationships in human muscles. An anatomical/functional argument for the existence of both. *Am J Phys Med* 62: 287–299, 1983.